Cyclic concentrator, carpet cloaks and fisheye lens via transformation plasmonics

2016 J. Opt. 18 044023

(http://iopscience.iop.org/2040-8986/18/4/044023)

OPEN ACCESS
IOP Publishing
Journal of Optics
J. Opt. **18** (2016) 044023 (16pp)
doi:10.1088/2040-8978/18/4/044023

Cyclic concentrator, carpet cloaks and fisheye lens via transformation plasmonics

M Alaoui[1], K Rustomji[1,2], T M Chang[1], G Tayeb[1], P Sabouroux[1], R Quidant[3], S Enoch[1], S Guenneau[1] and R Abdeddaim[1]

[1] Aix-Marseille Université, CNRS, Centrale Marseille, Institut Fresnel, Avenue Escadrille Normandie Niemen, 13013 Marseille, France
[2] Centre for Ultrahigh-bandwidth Devices for Optical Systems (CUDOS), University of Sydney NSW 2006, Australia
[3] ICFO—The Institute of Photonic Sciences, Mediterranean Technology Park Av. Carl Friedrich Gauss, 308860 Castelldefels (Barcelona), Spain

E-mail: sebastien.guenneau@fresnel.fr

Received 7 October 2015, revised 1 December 2015
Accepted for publication 2 December 2015
Published 1 April 2016

Abstract

We first review basic equations of plasmonics in anisotropic media. We recall the origin of Maxwell's gradient index fisheye lens. We then apply tools of transformation optics to the design of a cyclic concentrator and a variety of plasmonic carpet-cloaks. We further give a brief account of the discovery of spoof plasmon polaritons (SfPPs) by Pendry *et al* (2004 *Science* **305** 847–8) 150 years after Maxwell invented the fisheye lens. Finally, we experimentally demonstrate a concept of a fisheye lens for SfPPs at microwave frequencies. We stress that perfect metal surfaces perforated with dielectrics offer a playground for moulding surface waves in many areas of physics.

Keywords: transformation optics, plasmonics, metamaterials, spoof plasmons, microwaves, effective medium, lensing

(Some figures may appear in colour only in the online journal)

1. Introduction

Mathematicians and physicists have studied the physics of waves at structured interfaces for more than a century. In 1898 the mathematician Lamb (who gave his name to flexural waves in plates) wrote a paper on reflection and transmission through metallic gratings [1] which could be viewed as an ancestor of the 2004 theoretical proposal of spoof plasmon polaritons (SfPPs) by Pendry, Martin-Moreno and Garcia-Vidal [2]. SfPPs have been at the core of many exciting new developments in the past decade with the emergence of metamaterials in plasmonics [3–5] but also metamaterials to mould surface water waves, Lamb waves in structured plates and very recently surface seismic (Rayleigh) waves [6]. Indeed, ideas in so-called transformational plasmonics translate into the world of hydrodynamic and elastodynamic waves. This makes the class of surface electromagnetic waves known as surface plasmon polaritons (SPPs), which can be thought of as collective motions of electrons at structured metal/dielectric interfaces, a unique platform for the investigation of analogous phenomena in large-scale metamaterials, such as ocean wave and seismic metamaterials. Of course, one can argue that transformational plasmonics opens up unprecedented avenues for scaling down optical devices and it makes possible two-dimensional integrated optics capable of supporting both light and electrons with an accurate control of their flow. This in itself fully justifies the keen interest of the metamaterials community in this young topic that appeared in 2010. But while most efforts have so far focused on the extrapolation of concepts borrowed from guided optics to novel plasmonic functionalities, we would like to stress that most of what shall be discussed in the sequel finds some counterpart in the realm of linear (and possibly non-linear e.g.

tsunami) water waves and surface seismic waves. The plan of this paper is as follows. We first review basic equations of transformation plasmonics (TP). As a first application of TP (this versatile mathematical toolbox can be seen as a subset of transformation optics), we then propose to design a cyclic SPP concentrator and an omnidirectional SPP carpet cloak, inspired by the famous strategy of Li and Pendry of hiding under a carpet [7]. We then introduce a plasmonic fisheye, counterpart of Maxwell's fisheye in optics [8] (which was revisited by Luneburg [9] with an approach that could be considered as some ancestor of transformation optics) that we experimentally demonstrate by designing a metal grid supporting a spoof plasmon polariton in the microwave regime. We conclude the paper with remarks on potential applications of these concepts in the realm of ocean and seismic waves.

1.1. Mathematical tools of transformational optics applied to plasmonics

A few words on the mathematical setup should be in order if one wants to understand the specificity of a transformation plasmonics design in comparison with transformational optics. To simplify the discussion, we consider transverse magnetic (*p*-polarized) SPPs propagating in the positive *x*-direction at a flat interface $z = 0$ between metal ($z < 0$) and an isotropic medium ($z > 0$):

$$\begin{cases} H_2 = (0, H_{y2}, 0)\exp\{\mathrm{i}(k_{x2} - \omega t) - k_{z2}z\},\ z > 0 \\ H_1 = (0, H_{y1}, 0)\exp\{\mathrm{i}(k_{x1} - \omega t) + k_{z1}z\},\ z < 0 \end{cases}.$$

Note here that $R_e(k_{z1})$ and $R_e(k_{z2})$ are strictly positive in order to enforce the evanescence of fields above and below the interface $z = 0$.

Such fields are a solution of Maxwell's equations, therefore continuity of their tangential components is required across the interface $z = 0$, which translates into mathematics as $k_{x1} = k_{x2} = k_x$ and this in turn leads us to the famous dispersion relations for *p*-polarized SPPs:

$$k_{zi} = \sqrt{k_x^2 - \varepsilon_i\left(\frac{\omega}{c}\right)^2}, \quad \frac{k_{z1}}{\varepsilon_1} + \frac{k_{z2}}{\varepsilon_2} = 0,$$

where c is the speed of light in a vacuum, $\varepsilon_1(x, y) > 1 (z > 0)$, and $\varepsilon_2 = 1 - \frac{\omega_p^2}{\omega^2 + \mathrm{i}\gamma\omega}$, the usual Drude form in the metal ($z < 0$), for which ω_p is the plasma frequency (2175 THz) of the free electron gas and γ is a characteristic collision frequency of about 4.35 THz [3–5]. Actually, we note that since k_{z1} and k_{z2} are strictly positive SPPs can only exist if ε_1 and ε_2 are of opposite signs. One has:

$$k_x = \frac{\omega}{c}\sqrt{\frac{\varepsilon_1\varepsilon_2}{\varepsilon_1 + \varepsilon_2}},$$

which should be satisfied for SPPs to be able to propagate at the flat interface. SPPs are bound to the interface, and hence do not belong to the radiative spectrum (unlike leaky waves). Now, if one introduces a perturbation on the profile of the flat surface, for instance a bump, SPPs move to the radiative spectrum and so leakage cannot be avoided.

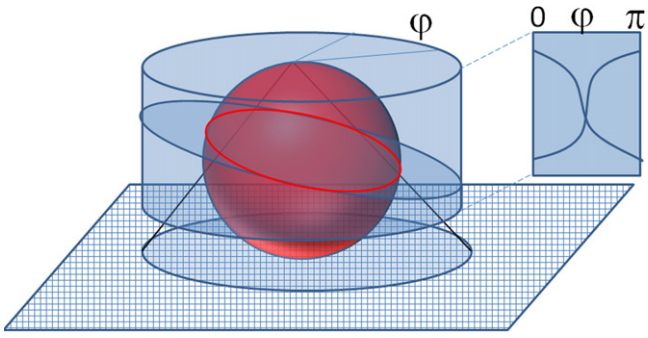

Figure 1. Mercator projection mapping each point on the surface of a sphere to a projected point (φ, u) on the surface of a cylinder. A line is drawn through each point on the surface of the sphere. The image is the point where the line intersects the cylinder. The projection of a great circle on the surface of the sphere (red) is an ellipse on the cylinder (blue). Unfolding the surface of the cylinder (see right inset), the trajectory of light in physical space is indicated by the blue lines. The surface development of the image on the cylinder reveals the typical profile of ray trajectories on the plane (cosine function) and the position of the image (intersection of the curves).

However, if we now analyze the propagation of SPPs at a flat interface between an anisotropic heterogeneous medium described by diagonal tensors of relative permittivity and permeability $\underline{\underline{\varepsilon'}} = \mathrm{diag}(\varepsilon_{xx2}, \varepsilon_{yy2}, \varepsilon_{zz2})$ and $\underline{\underline{\mu'}} = \mathrm{diag}(\mu_{xx2}, \mu_{yy2}, \mu_{zz2})$ (where the tensor components depend upon space variables) and a metal, the same derivation as above shows that equation the dispersion relation of SPPs takes the following form [10]:

$$k_x = \frac{\omega}{c}\sqrt{\frac{\varepsilon_{zz2}\varepsilon_1(\mu_{yy2}\varepsilon_1 - \varepsilon_{xx2})}{\varepsilon_1^2 - \varepsilon_{xx2}\varepsilon_{zz2}}}.$$

This equation shows that one now has additional degrees of freedom to mould the flow of SPPs at interfaces between metal and transformed dielectric media. An even richer dispersion relation can be obtained at an interface between transformed metal and dielectrics [11–14].

As an alternative to the control of SPPs on flat interfaces between transformed media, one might wish to consider curved interfaces. The groups of Martin-Moreno and Garcia-Vidal [11] and Zhang [12] have explored this fascinating route. To conclude this introduction, we would like to stress that in a similar way to what transformation optics has achieved with antennas, lenses, carpets, cloaks, concentrators, beam-splitters, super-scatterers, optical black holes etc for volume electromagnetic waves in specially designed anisotropic heterogeneous media, transformation plasmonics opens a door to a whole new world of metamaterials for light harvesting in surface science.

1.2. Mapping a virtual sphere on plasmonic surfaces

It is well known that the geodesics on a sphere surface are the great circles. As illustrated by the red line in figure 1, this implies that all geodesics passing through a point should cross at the same point on the opposite side. Transformation media have been designed for electromagnetic waves in order to mimic the sphere surface. One famous example of an optical system within which light follows the same trajectories as it

would on a sphere is the fisheye lens, which was conceived 160 years ago by James Clerk Maxwell. One might hastily conclude that transformation optics (TO) takes its roots in the 19th century. However, at that time Maxwell did not use TO tools to deduce the spatially varying refractive index of the eponymous fisheye lens: mathematical objects underpinning TO such as tensors would be used by Albert Einstein more than half a century afterwards in the context of general relativity.

Although light rays in the designed transformation medium experience the same focusing phenomenon as on a sphere surface, in the mathematical problem Maxwell proposed (see below), he did not consider any stereographic projection of the sphere surface on the plane where light propagates along circular trajectories (cf problem 3, vol 8 in [8]):

A transparent medium is such that the path of a ray of light within it is a given circle, the index of refraction being a function of the distance from a given point in the plane of the circle. Find the form of this function and shew that for light of the same refrangibility:

(1) The path of every ray within the medium is a circle.
(2) All the rays proceeding from any point in the medium will meet accurately in another point.
(3) If rays diverge from a point without the medium and enter it through a spherical surface having that point for its centre, they will be made to converge accurately to a point within the medium.

Maxwell notes that his solution to this problem (based on Euclidean geometry) came from:

The possibility of the existence of a medium of this kind possessing remarkable optical properties, was suggested by the contemplation of the structure of the crystalline lens in fish; and the method of searching for these properties was deduced by analogy from Newton's Principe, lib. I., prop. vii.

The realization that the solution to this problem could be produced via a completely different route [9], nowadays called transformation optics, came 90 years after Maxwell posed his mathematical problem. Depending upon how one projects the points of the sphere on a flat surface (e.g. a cylinder or a plane) one can achieve a cyclic lens or a fisheye. The paper is now devoted to such applications, together with more elaborate, invisibility cloak and carpet, metamaterials.

2. Plasmonic cyclic concentrator

Let us start with the projection of the surface of a sphere on a cylinder. This amounts to considering a refractive index with a hyperbolic secant profile:

$$n(r) = n_0 \,\mathrm{sech}(\alpha r) \text{ where } \alpha = \frac{1}{R_0}\cosh^{-1}\frac{n_0}{n_R}$$

where R_0 is the radius of the cylindrical lens, and n_0 and n_R are respectively the refractive indices (invariant along the z-axis) at $r = 0$ (along the optical axis) and at $r = R_0$ (at the outer edge of the lens). Such a design can be deduced from quasi-conformal grids.

We would like to propose a structured design of a cyclic concentrator, which mimics the transformed design of such an ideal quasi-conformal grid. We note that the effective permittivity ε_e of most two-phase composite media is given by the classical Maxwell–Garnett formula:

$$\frac{\varepsilon_e - \varepsilon}{\varepsilon_e + \varepsilon} = \frac{\varepsilon_0 - \varepsilon}{\varepsilon_0 + \varepsilon} f$$

where ε_0 and ε are the permittivity of material (in our case PMMA) and background (Air), respectively. We consider that the filling fraction f which is equal to the ratio of cross-section area of material (PMMA) to the elementary cell is that of a hexagonal unit cell (figure 2); thus $f = 1 - (4\pi/\sqrt{3})^*(\mathrm{r/d})^2$ with r the radius of air holes. The concentrator consists of air holes of diameters ranging from 128 nm to 340 nm and the size of each elementary cell is d = 267 nm.

2.1. Analysis of focusing properties of an elementary cell of the cyclic concentrator

Computing the electromagnetic field for a plane wave incident on the structured concentrator described in figure 2 (using the commercial finite element software COMSOL MULTIPHYSICS), we note in figure 3 that the energy is concentrated at the exit of the lens, and this corresponds to the focusing point in figure 1.

2.2. Analysis of focusing properties of the cyclic concentrator

Let us now increase the length of the concentrator in order to achieve multiple focusing points as suggested by figure 1. We note in figure 4 that the energy is concentrated cyclically along the optical axis. In addition, our device works over a large bandwidth (see figure 5) as its structured design is based upon an effective medium theory.

3. Plasmonic carpet-cloaks

The first example of a cylindrical invisibility cloak for SPPs deduced from Pendry's coordinate transformation [15] was proposed by some of us [9]. Let us recall briefly its design: one need consider an electromagnetic space described by cylindrical coordinates (r', θ', z') where the cloak's inner boundary is chosen to be $r' = a$ and the outer boundary is $r' = b$. Then, a coordinate transformation is applied to transform (r', θ', z') to (r, θ, z) where the corona $a < r' < b$ is mapped onto a disk $0 < r < b$. Following [15] the inverse of such a transformation is:

$$r' = \begin{cases} \dfrac{b-a}{b} r + a, & r' \leqslant b, \\ r, & r' > b \end{cases} \theta' = \theta,\ \varphi' = \varphi$$

Under such an inverse transformation, the region $r' < b$ is compressed to the region $a < r < b$. It has been established

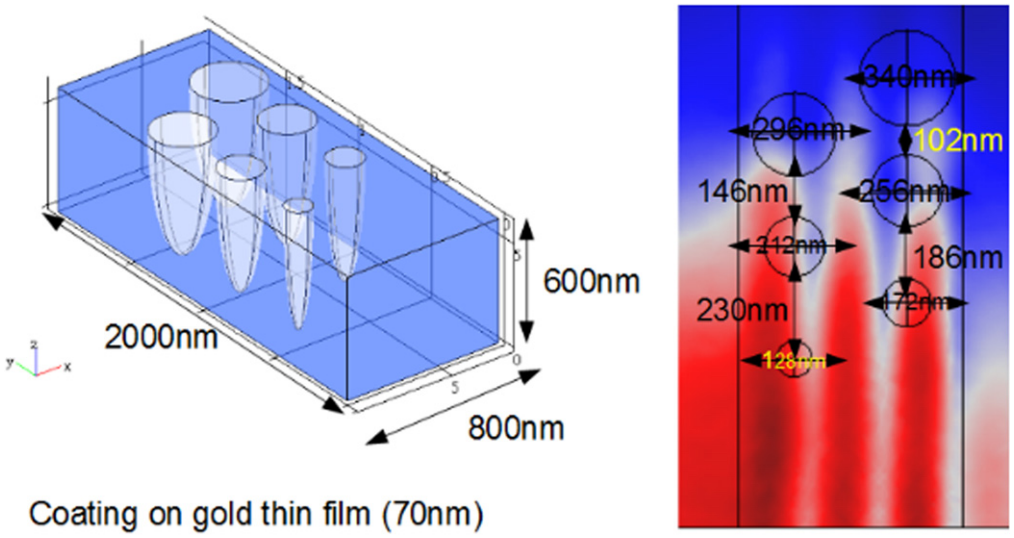

Figure 2. (Left) Three-dimensional diagrammatic view of one cell of a structured cyclic concentrator. (Right) Top view, where the numbers denote the radii of air holes.

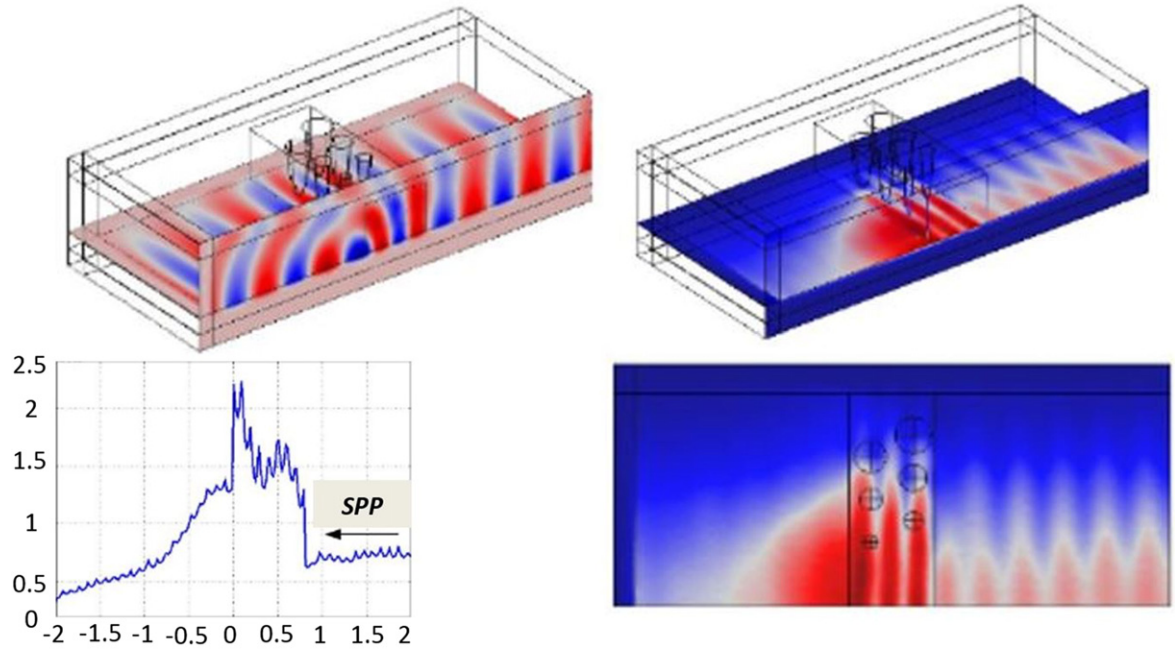

Figure 3. Numerical validation at wavelength $\lambda = 800$ nm for one cell of a cyclic concentrator. (Lower left) Total energy density variation along the optical axis; (upper left) three-dimensional plot of the real part of the y-component of magnetic field; (upper right) norm of magnetic field; (lower right) top view of norm of magnetic field.

that the material parameters of the invisibility cloak expressed in cylindrical coordinates are given by:

$$\varepsilon_r = \mu_r = \frac{r-a}{r}, \varepsilon_\theta = \mu_\theta = \frac{r}{r-a},$$
$$\varepsilon_z = \mu_z = \left(\frac{b}{b-a}\right)^2 \frac{r-a}{r}.$$

One can see that such a design requires strongly anisotropic tensors of permittivity and permeability, so the dispersion relation of the SPP is given by the general formula of section 1.1. A numerical simulation is performed with COMSOL MULTIPHYSICS for such parameters and shown in figure 6.

The implementation of such an invisibility cloak is fairly challenging; we therefore go back to spatially varying, scalar-valued, refractive index metamaterials.

3.1. SPP carpet-cloak constructed with quasi-grids

Let us now investigate the application of quasi-grids that preserve right angles in transformed metrics i.e. avoid the use of artificial anisotropy in the metamaterials' designs. In 2010, some of us introduced the design of a broadband plasmonic

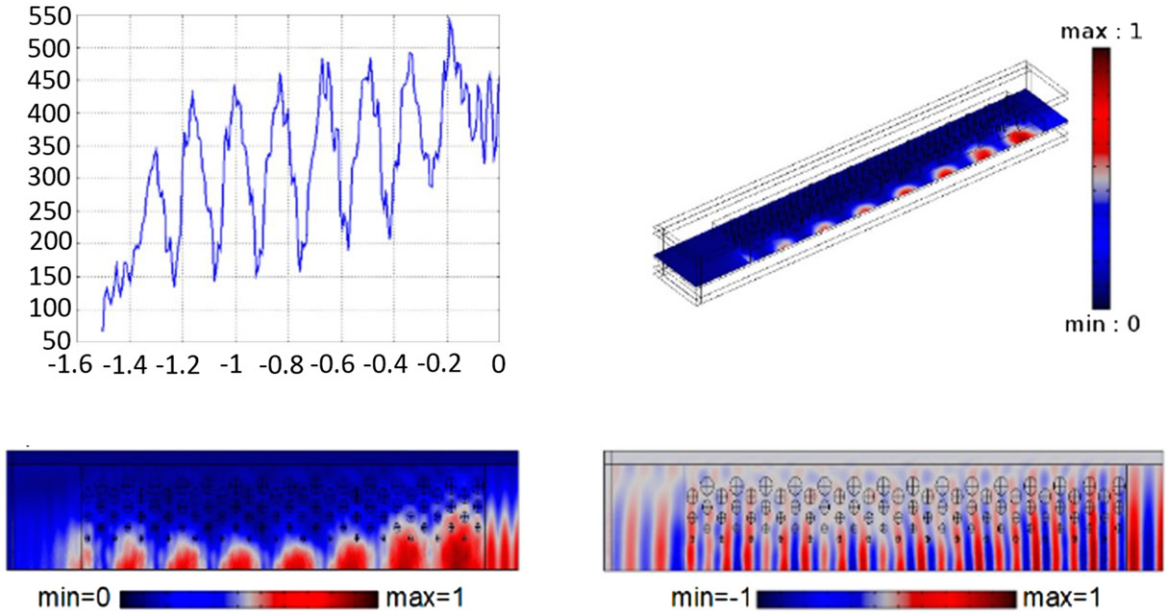

Figure 4. Numerical validation at wavelength $\lambda = 800$ nm for a cyclic concentrator (with 15 cells) of length 1.5 μm and width of 4 μm. (Upper left) Electric field norm with cyclic concentration along the optical axis (upper left); (upper right) three-dimensional plot of the total energy density. Finally, the slice of the plot of the norm (lower left) and the z-component (lower right) of the electric field in the horizontal plane show the focusing effect.

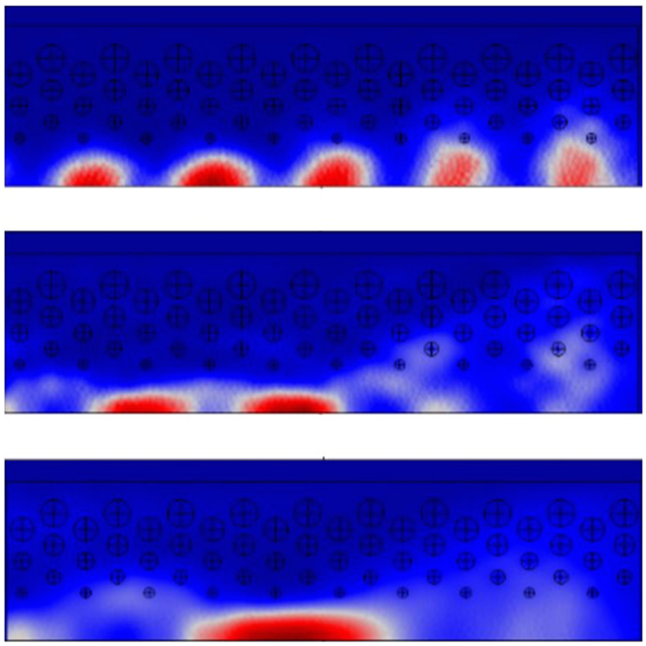

Figure 5. Total energy density in cyclic concentrator for wavelengths of (top) 800 nm; (middle) 1000 nm; (bottom) 1550 nm. One notes the cyclic concentration occurs at short wavelengths.

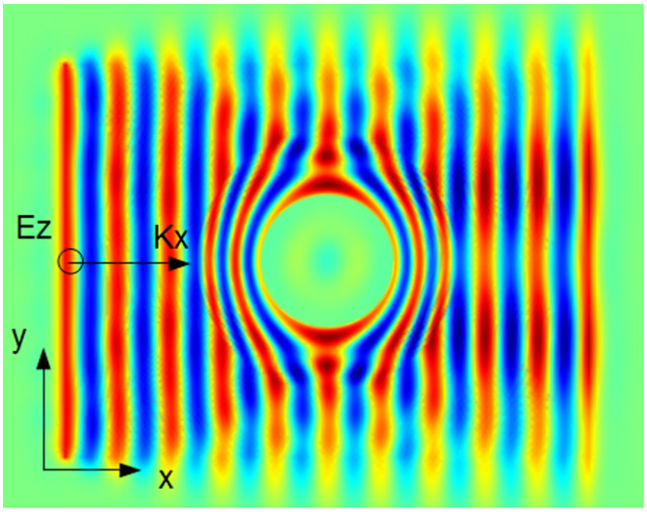

Figure 6. An incident SPP plane wave (wavelength $\lambda = 800$ nm, s-polarized) propagates (from left to right) through an invisibility cloak (3000 nm in diameter). One notes the field vanishes in the centre. Top view showing the real part of longitudinal electric field E_z (with linear colour scale from blue to red, from negative to positive values with green for zero).

carpet [13]. In figure 7, we show a finite element numerical computation performed by Muamer Kadic within the framework of his PhD thesis at Institut Fresnel in 2010 that clearly demonstrates the nearly flat wavefront for a plane SPP wave incident upon a curved mirror at 700 nm. However, such an invisibility effect is achieved thanks to high refractive index pillars deposited at the nodes of a quasi-grid on a metal surface.

In order to meet experimentally the parameters found in Kadic's simulations, Jan Renger (one of the researchers in Quidant's group at ICFO) chose a configuration in which a gold surface is structured with TiO_2 nanostructures. The TiO_2 pillars forming the crescent-moon-like carpet were first fabricated on top of a 60 nm thin Au film by combining electron-beam lithography and reactive ion etching. In a second lithography step, Jan Renger added a curved Bragg-type reflector (formed by 15 gold lines (section = 150 nm $\times$ 150 nm) periodically separated by half of the SPP

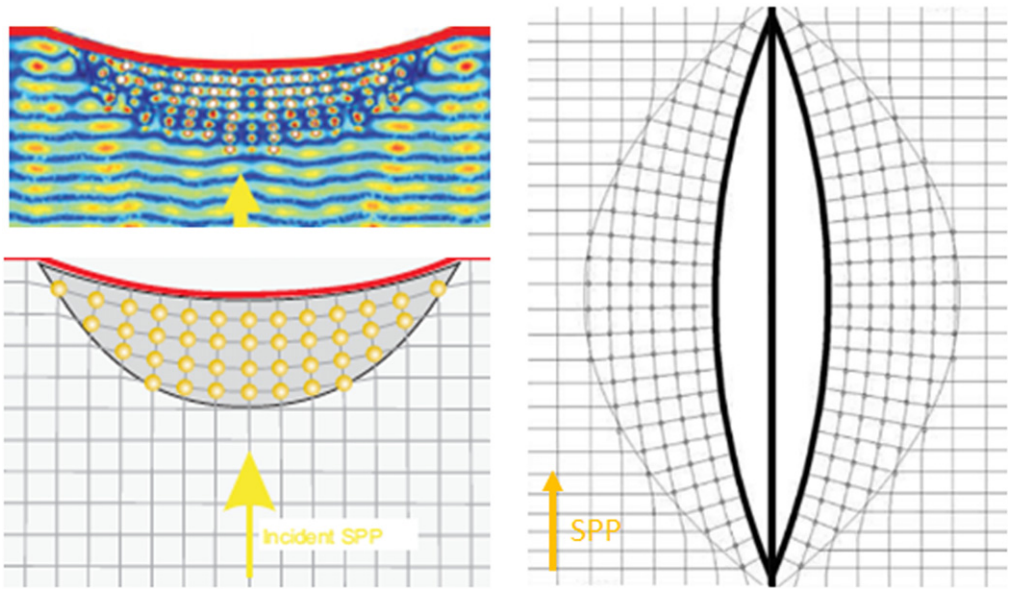

Figure 7. From plasmonic carpet to unidirectional cloak: an invisibility carpet deduced from a quasi-conformal grid (left) that serves as a basis for a unidirectional SPP cloak (right). Note that the direction of propagation of SPP has been tilted through an angle of $\pi/4$ in the SPP cloak. SPP carpet has been designed and by Muamer Kadic and experimentally tested by Jan Renger [13].

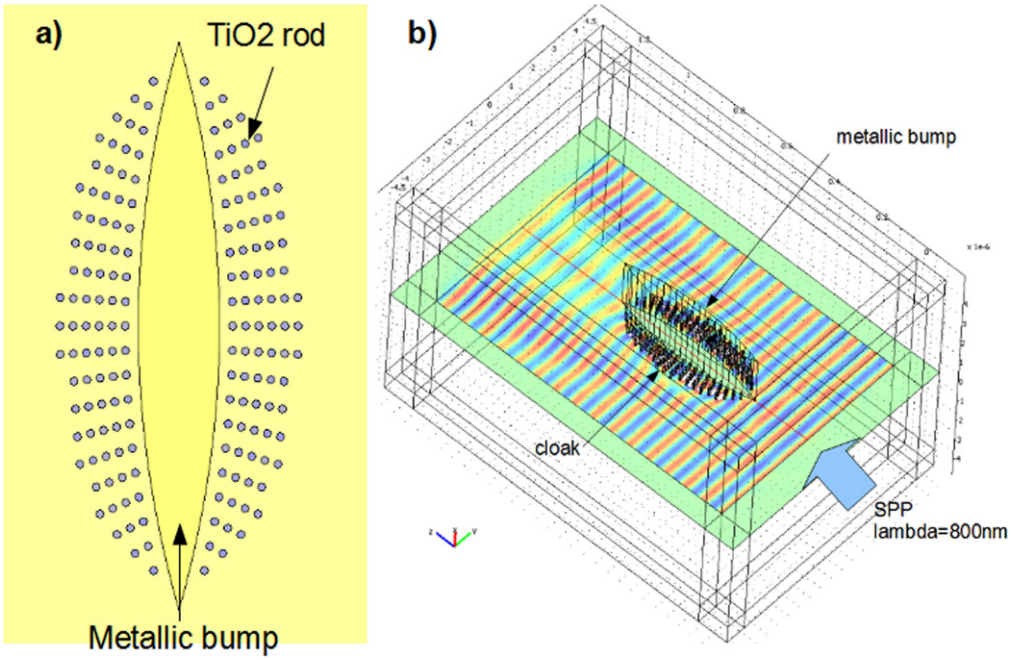

Figure 8. Plasmonic unidirectional cloak. (a) Design of the SPP cloak with TiO_2 rods on a metal surface; (b) simulation of the scattering by an SPP with perfectly matched layers implemented on either sides of the computational domain.

wavelength), acting as the object to be hidden behind the carpet. The shape of the obtained TiO_2 particles is conical ($h = 200$ nm, $r = 100$ nm) as a consequence of the etching anisotropy, but the reported experimentally characterized efficiency of the carpet was quite convincing (reduction of scattering up to a factor 3.5 throughout the 700 nm to 900 nm wavelength range) at that time [13]. We would like to revive this successful design of SPP carpet as a uni-directional SPP cloak, as proposed in figure 7(right).

What we have done is to simply consider a combination of two SPP carpets, which we have stuck together, creating a pinched, uni-directional cloak. The parameters used in the COMSOL computation reported in figure 8 are those of figure 8 except that there are twice as many rods, and the SPP should now be incident on the cloak from the side. We place a metallic bump that fills the invisibility region, and we check the scattering by the metallic bump with and without the cloak; see figure 9.

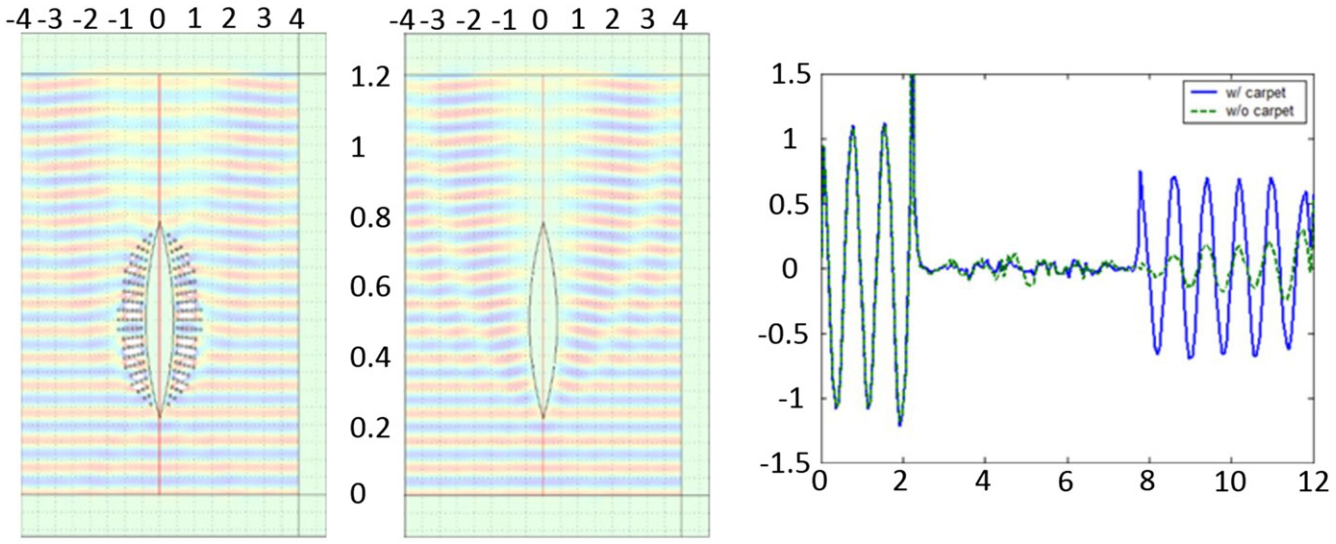

Figure 9. Plasmonic unidirectional cloak. (Left) Scattering by a metallic bump surrounded by the SPP cloak with TiO_2 rods on a metal surface; (middle) same without cloak; (right) profile of real part of longitudinal electric field E_z with (blue curve) and without (green curve) the carpet.

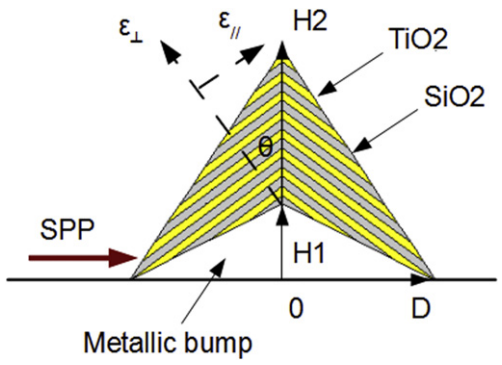

Figure 10. Schematic of the proposed homogeneous cloak achieved with a layered medium. Here $\varepsilon\perp$ and $\varepsilon_{//}$ represent the permittivity entries in the two principle axes.

perpendicular to the cloak device) polarization can be expressed as

$$\bar{\bar{\varepsilon}} = \begin{bmatrix} \left(\frac{H_2}{H_2 - H_1}\right)^2 & \pm\left(\frac{H_2}{H_2 - H_1}\right) \\ \pm\left(\frac{H_2}{H_2 - H_1}\right)^2 \frac{H_1}{D} & 1 + \left(\frac{H_2}{H_2 - H_1}\right)^2 \left(\frac{H_1}{D}\right)^2 \end{bmatrix}$$

where H_1 and H_2 represent the heights of the obstacle and the cloak, respectively, and D is half the bottom length of the cloak. The permittivity tensor of the above problem can be deduced by rotating the optical axis through an angle θ:

$$\begin{bmatrix} \varepsilon_{\|} & 0 \\ 0 & \varepsilon_{\perp} \end{bmatrix}.$$

According to the effective medium theory, the anisotropic parameters can be achieved with an alternation of layered materials at sub-wavelength scale.

Therefore, appropriately combining two dielectric layers with permittivities ε_1 and ε_2 would yield the material with desired effective permittivity:

$$\varepsilon_{\|} = r\varepsilon_1 + (1 - r)\varepsilon_2$$

and

$$\varepsilon_{\perp} = \frac{\varepsilon_1\varepsilon_2}{r\varepsilon_2 + (1 - r)\varepsilon_1}$$

where r denotes the filling factor of the constituent materials.

To illustrate how SPPs interact with this structure, we simulate in figure 11 its propagation along a metal bump on a metal surface (upper panel), the same obstacle cloaked with

3.2. Homogeneous SPP cloak constructed with uniform layered structures

We have successfully designed some carpet cloaks using quasi-grids. There is nonetheless another interesting route towards plasmonic carpets, using anisotropic media. This might prove harder to implement in practice, but for the sake of completeness we show below two possible designs in which the metal surface has defects in the transverse (vertical) direction, a case first studied by the groups of Garcia-Vidal in Madrid [11] and Zhang in Berkeley [12].

Let us first propose a layered carpet cloak with a uniform silicon grating structure. The cloak takes a triangular shape as shown in figure 10. The permittivity tensor of a non-magnetic cloak for transverse-magnetic (TM, magnetic field

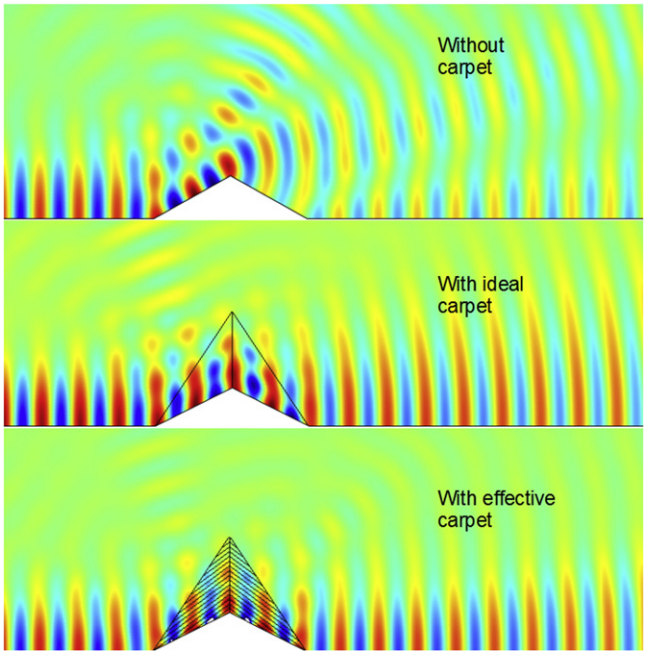

Figure 11. From top to bottom: bare protruded plane, cloaked protruded plane with ideal carpet, and layered carpet respectively. The incident wavelength is 800 nm.

an ideal carpet (middle panel) and with a layered carpet (lower panel).

In fact, as announced before, there is another interesting possibility for a plasmonic carpet. One can consider rods instead of homogeneous layers, following the route of quasi-conformal mapping. The point is again to avoid dealing with anisotropy. The quasi-grid is in the transverse (vertical) plane, and placing high refractive index rods at its nodes as shown in figures 12 and 13 allows us to control surface plasmon polaritons (SPPs) and volume electromagnetic waves. In fact, as already pointed out in [14], transformation optics and plasmonics sometimes lead to the same designs in the case of carpets. This does not come as a surprise since surface electromagnetic waves are solutions of Maxwell's equations.

4. Theory of spoof plasmons and Maxwell's fisheye

In this last section, we would like to experimentally demonstrate some designs of a Maxwell fisheye deduced from a stereographic projection as shown in figure 1. The fabrication of this gradient index lens would be hard to achieve in the range of visible wavelengths, hence we turn our attention to microwaves. It is well known that conditions for the existence of SPPs cannot be met at microwaves. However, thanks to the proposal of surface spoof plasmon polaritons (SfPPs) on structured perfect metal surfaces [2] we know there is a natural path towards the design of transformation-based plasmonic metamaterials in the microwave regimes. We can thus simulate and experimentally characterize a Maxwell fisheye for SfPPs at Institut Fresnel. To do this, we first follow the recipe in the seminal paper by Pendry, Martin-Moreno and Garcia-Vidal [2] in order to generate a spoof plasmon source.

4.1. Introduction to spoof plasmon polaritons

Let us recall the main steps of the SfPPs' derivation as proposed by Pendry and his Madrilenian colleagues in [2] where all the details can be found (we note in passing that some elements of the mathematical proof of what we might call the *SfPP's existence theorem* are analogous to equations in a book chapter on grating anomalies by Daniel Maystre [18]). Assuming that the incident wave wavelength is much larger than the sidelength of square perforations (say, a), and array pitch (say, d), that is $a < d \ll \lambda_0$, see figure 14, one can use homogenization techniques to derive the effective dispersion relation of SfPPs in the following manner. Notice first that the incident field excites mostly the fundamental mode of each waveguide within the periodically perforated metal (the electromagnetic field vanishes inside the perfect metal parts). In each dielectric waveguide one has:

$$E = E_0\,[0,1,0]\sin\left(\frac{\pi x}{a}\right)\mathrm{e}^{\mathrm{i}(k_z z-\omega t)} \times 0 < x < a \text{ and } 0 < y < a$$

with the z-component of the wave vector such that:

$$k_z = \mathrm{i}\sqrt{\frac{\pi^2}{a^2} - \mu_h\varepsilon_h {k_0}^2}.$$

Here, k_0 is the wavenumber in a vacuum and ε_h and μ_h are the permittivity and permeability of the dielectric waveguides (for our experiments, we shall choose sand).

Note that for long wavelengths, due to symmetry, the effective tensors of permittivity and permeability of the periodic set of square waveguides satisfy ε_z, $\varepsilon_x = \varepsilon_y$ and μ_z, $\mu_x = \mu_y$. Moreover, it is well known in the homogenization of perfect metal–dielectric structures [16, 17] that

$$\varepsilon_z = \mu_z = \infty.$$

As noted by Pendry *et al* in their original derivation, it seems reasonable to assume that the effective field inside the perforated metal can be written as:

$$E' = E'_0\,[0,1,0]\mathrm{e}^{\mathrm{i}(k_z z + k_x x-\omega t)}$$

so that identifying incident and reflected wave-fields, and using the tangential continuity of the averaged electromagnetic field at the interface between air and structured metal–dielectric medium, one finds that

$$(E_* H)z = \frac{-k_z E_0^2 a}{\omega\mu_h\mu_0 d^2}\int_0^a \sin^2\left(\frac{\pi x}{a}\right)\mathrm{d}x = \frac{-k_z E_0^2 a}{\omega\mu_h\mu_0 2d^2}$$
$$= (E'_* H')_z = \frac{-k_z E_0'^2}{\omega\mu_h\mu_x}.$$

It follows that the effective permeability tensor entries are:

$$\mu_y = \mu_x = \frac{2d^2\mu_h}{a^2}\left[\frac{2a^2}{\pi d^2}\right]^2 = \frac{8a^2\mu_h}{\pi^2 d^2}.$$

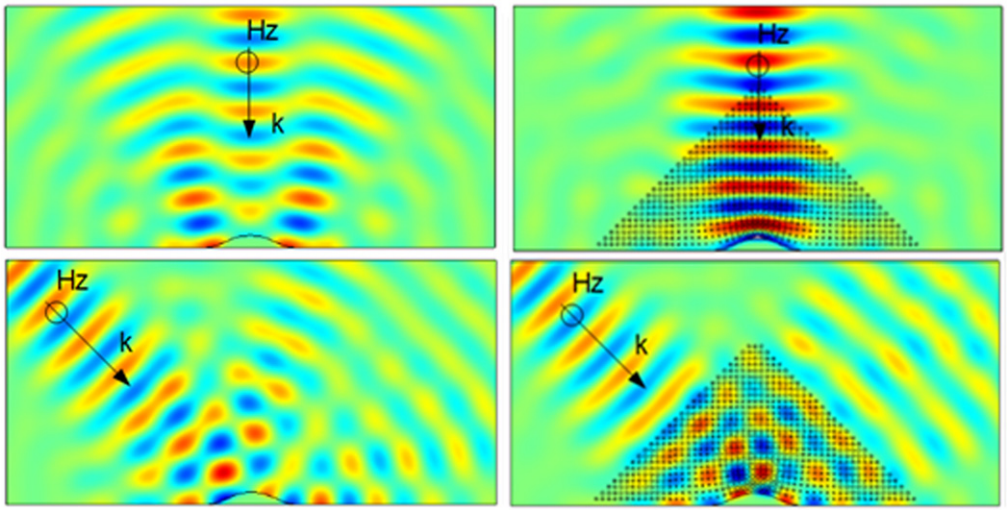

Figure 12. Scattering of an incident Gaussian beam by a metallic bump on its own (left) and dressed with a carpet (right). The incident wavelength is 800 nm and its angle made with the normal to the interface has been varied between 0 (normal incidence) to 45°.

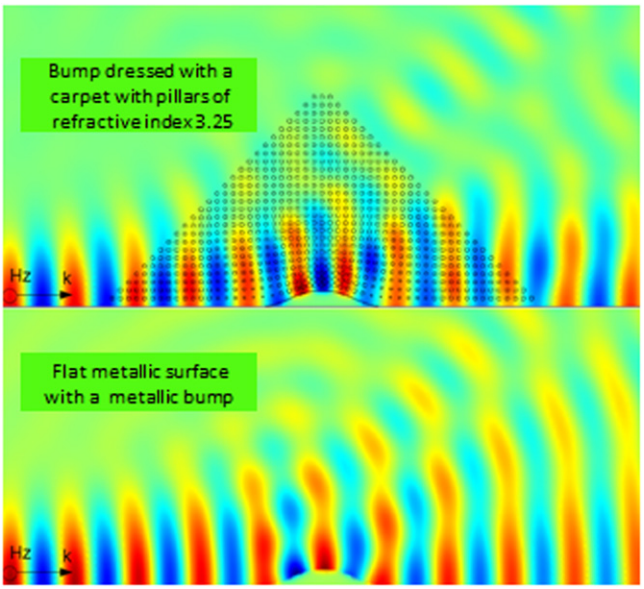

Figure 13. Propagation of SPP at 800 nm on the same metal surface as in figure 12.

$$\text{Aside from that } k_z = k_0\sqrt{\mu_y\varepsilon_x} = \mathrm{i}\sqrt{\frac{\pi^2}{a^2} - \mu_h\varepsilon_h {k_0}^2}$$

so that the effective permeability tensor entries have the form:

$$\varepsilon_y = \varepsilon_x = \frac{1}{\mu_x}\left(\varepsilon_h\mu_h - \frac{\pi^2}{a^2{k_0}^2}\right) = \frac{\pi^2 d^2\varepsilon_h}{8a^2} \times\left(1 - \frac{\pi^2{c_0}^2}{\varepsilon_h\mu_h a^2\omega^2}\right)$$

with c_0 the celerity of light in a vacuum.

Pendry, Martin-Moreno and Garcia-Vidal concluded from this asymptotic analysis that effective parameters are reminiscent of low-frequency plasmons in highly conducting wired media [18–23] except that $\omega_p = \frac{\pi c_0}{a\sqrt{\varepsilon_h\mu_h}}$ is the cut-off frequency of square waveguides in the perforated metal; see figure 15.

In fact, any metal surface structured by a periodic array on a subwavelength scale can be described by such a low-frequency plasmon resonance and would support a spoof plasmon. In the case of dielectric waveguides of an arbitrary cross section, ω_p has a slightly more complex expression, but the structure of the effective tensors of permittivity and permeability remains essentially the same (the z-component is infinite) although ε_x differs from ε_y (as well as from μ_x and μ_y) so that one essentially adds artificial anisotropy to the effective medium. A more general dispersion relation follows, along the lines of section 1.1.

4.2. Maxwell's fisheye in the spotlight

Inspired by John Pendry's revolutionary idea of a perfect lens via negative refraction [24], Ulf Leonhardt proposed, in a mathematically beautiful work, that a closed Maxwell fisheye lens (with a perfect mirror placed at a distance from the centre corresponding to the radius of a virtual sphere used in its design) might also be a good candidate for a lens with high resolution [25]. Some authors questioned this claim [26, 27] and [28] failed to observe subwavelength features in the image within the mirrored fisheye lens. Although a microwave experiment suggested some subwavelength nature of the image [29], Roberto Merlin has conclusively shown [30] that a passive drain considered by Leonhardt in [25] (which is nothing but a time-reversed source placed very close to the theoretical position of the image) is necessary in order to beat the Rayleigh diffraction limit in Maxwell's fisheye. Moreover, Merlin pointed out that in [29], the outlets were absorbers identical to the source and impedance matched to the cables, which thus behaved as sources in reverse. In fact evanescent waves, which are essential in Pendry's perfect lens, do not contribute to the image reconstruction in the mirrored Maxwell's fisheye. Actually, the original fisheye lens shares much of the optical properties of a spherical lens, and what Leonhardt added as a further smart twist to its design is reminiscent of time-reversal sources and cavities in

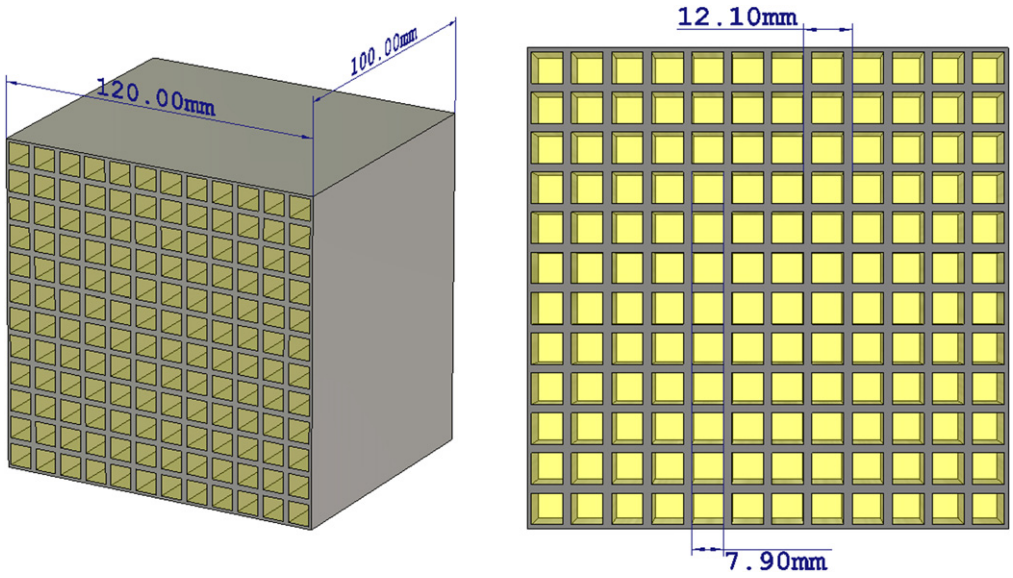

Figure 14. Perforated (perfect) metal. (Left) Three-dimensional view with dimensions of macroscopic plasmonic crystal. (Right) Top view with dimensions of microscopic periodic cell.

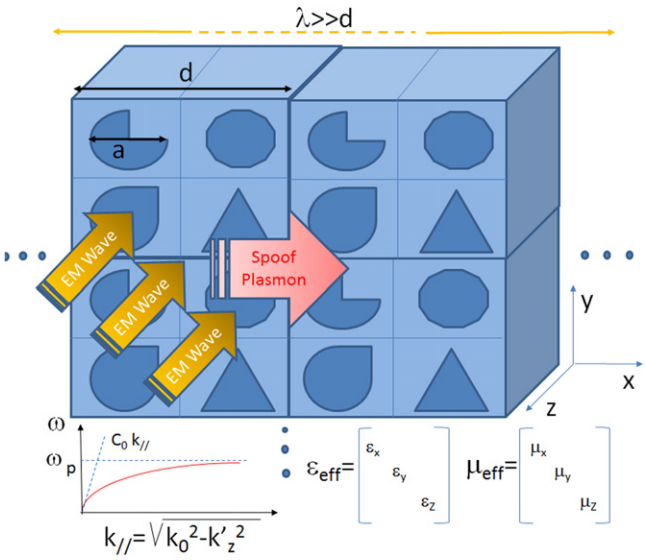

Figure 15. Schematics of Pendry, Martin-Moreno and Garcia-Vidal's proof of concept of spoof plasmon polaritons (SfPPs). A perfect metal surface structured with periodically arranged dielectric waveguides behaves in the long wavelength limit like an effective medium with permittivity and permeability tensors displaying some plasma frequency dependence in ε_x, ε_y (with infinite ε_z and μ_z). This makes possible some electromagnetic surface waves with a dispersion reminiscent of plasmon polaritons (its asymptotes are the light line at low frequency and the plasma frequency ω_p at large transverse wavenumbers $k_{//}$ in contrast to an isotropic plasma which has this asymptote shifted downwards by a factor of square root of 2. This makes SfPPs a new class of surface waves.

the work of Mathias Fink's group [31]. Nonetheless, let us stress that Leonhardt's paper has revived the interest of the wave community in Maxwell's lens, notably with some experiments performed in the time domain for elastic waves focusing on a fisheye-like plate [32].

The secret of the fisheye is a refractive index inversely proportional to a virtual sphere curvature. Indeed, if one considers a sphere of radius a lying on a plane, its stereographic projection leads to

$$n(r) = \frac{a^2 n_0}{a^2 + r^2} \quad \begin{cases} n = n_0 & \text{for} \quad r = 0 \\ n = 1 & \text{for} \quad r = a\sqrt{n_0 - 1} \end{cases}$$

with n_0 the refractive index at the centre of the lens. The stereographic projection of great circles on the sphere (geodesics of ray trajectories emitted by a source at a point that converge to an antipodal image point) actually leads to bipolar coordinates in the plane.

4.3. A fisheye for surface plasmon polaritons

Research scientists have shown a keen interest in the Maxwell fisheye in the past few years, and we have mentioned that its design has been translated to the area of elastic waves in plates [32]. This suggests that a similar design might hold in plasmonics. We tested the design of a plasmonic fisheye without boundaries (see figure 16) using COMSOL MULTIPHYSICS. It transpires from this figure that, in theory, one can focus SPP with such a lens. However, the required spatially varying refractive index requires some exotic medium that needs to be engineered.

Moreover, figure 16 shows some interesting features of field concentration at the antipodal location to the line source at the periphery of the lens that would need to be confirmed with a less challenging numerical model. We therefore decided to opt for a model of plasmonic fisheye within a cylindrical metallic cavity (indeed, in this case, there is no possible issue with perfectly matched layers that are quite subtle to implement for such a case). Figure 17 shows a structured design of fisheye surrounded by a metallic cavity. This design consists of TiO_2 pillar inclusions in air atop a

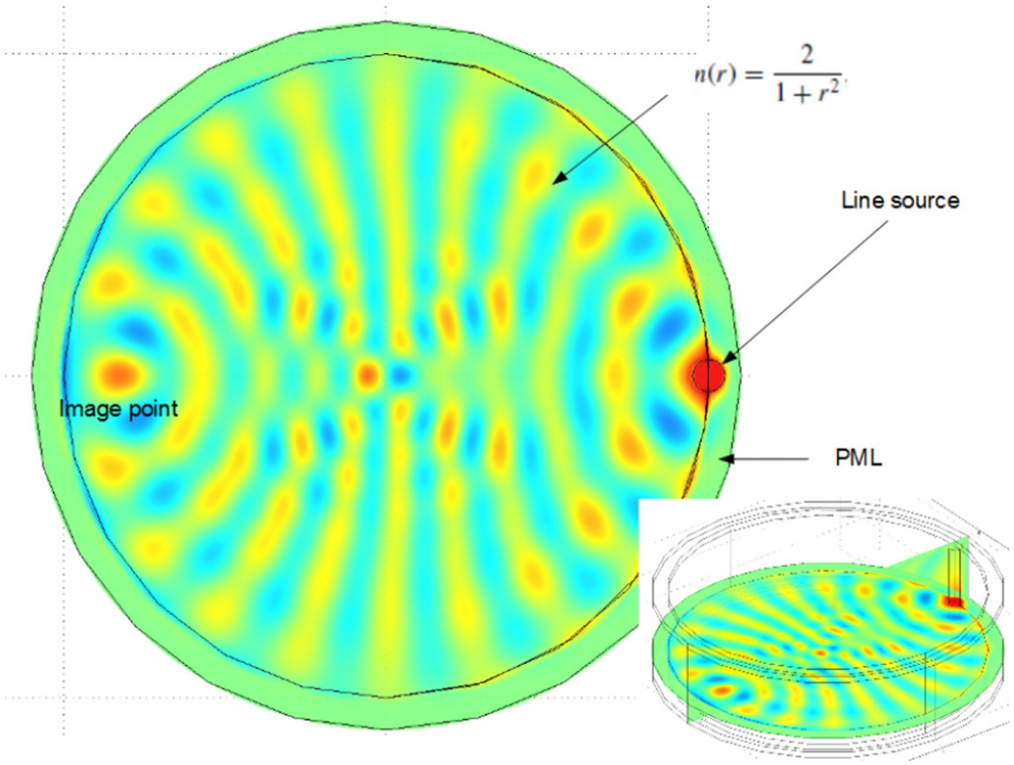

Figure 16. Numerical simulation for an open fisheye of radius 5 micrometers, one can focus SPP with such a lensn SPP at 1550 nm at position r_0 with a (diffraction limited) image observed almost at position $r_1 = -r_0$. Cylindrical perfectly matched layers (consisting of anisotropic absorptive medium above the interface and anisotropic metal below) are used to model the infinite extent along the radial direction.

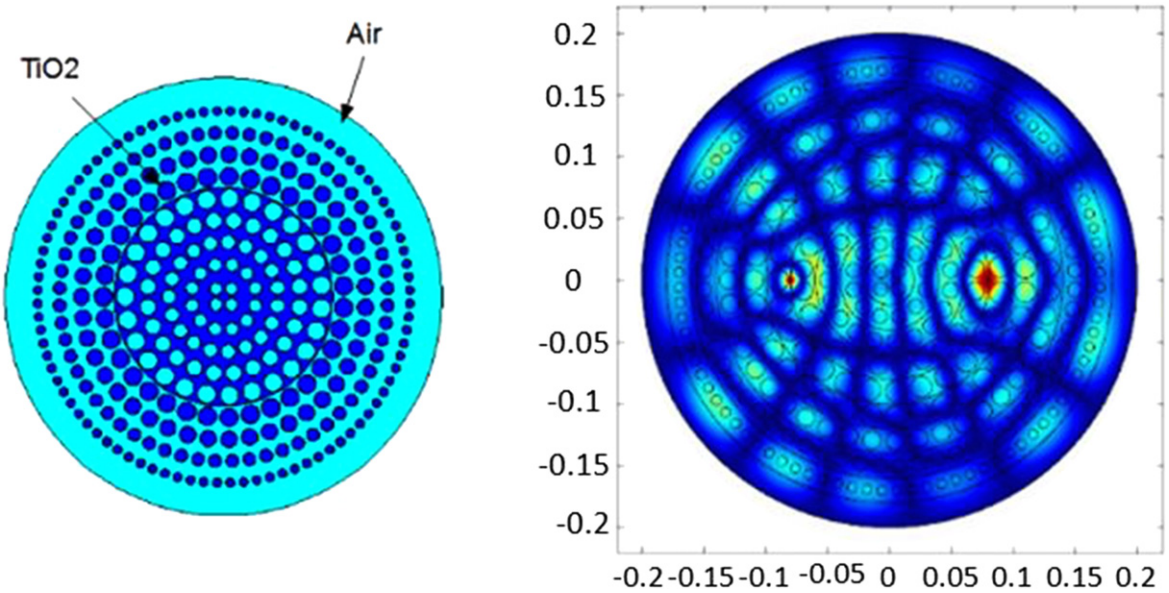

Figure 17. Numerical simulation for a closed fisheye placed atop a semi-infinite metal substrate (gold). A line source generates a SPP at position r_0 with a (diffraction limited) image observed almost at position $r_1 = -r_0$. (Left) Refractive index distribution: light blue and dark blue indicate air ($n = 1$) and TiO_2 ($n = 2.5$) respectively. (Right) Field intensity: the point source is located at $r_1 = 0.4R$ on the left side of the lens, with R the radius of the cylindrical metallic (perfect) cavity surrounding the fisheye. Wave wavelength is $0.575R$.

metal surface. The source is placed well within the lens (far from the metal cavity) and the image is formed at a location which can be deduced from ray optics considerations on the virtual sphere used to generate the Maxwell fisheye (through stereographic projection as we already discussed). This design will be a source of inspiration for our experimental realization of the plasmonic Maxwell fisheye for SfPPs, which comes next.

5. Microwave experiments on spoof plasmons and Maxwell's fisheye

5.1. A source of spoof plasmon polaritons

For our microwave experiments, we consider a plasmon frequency about 10 GHz ($f_c = 10$ GHz), which corresponds to a wavelength $\lambda_c = 3$ cm. Depending upon the medium which we consider within the dielectric inclusions of the metallic array, this will bring specific constraints on the cross-sectional size of inclusions and the array pitch, in order to meet the long wavelength criterion $a < d < \lambda_c$. In fact, homogenization theory requires that λ_c be much larger than d but in practice it is sufficient to have a wave wavelength three times larger than the array pitch.

If we consider air inclusions ($n = 1$), we find that $a = 15$ mm, $d = 30$ mm meets the homogenization criterion. For dry sand inclusions (modelled with $n = 3.6$, as checked with the *EpsiMu*® tool developed at Institut Fresnel which consists of a coaxial measuring cell and a dedicated software; see [34, 35]), we can take $a = 7.9$ mm, $d = 10$ mm. We then used the CST Microwave studio commercial package to generate the dispersion diagram associated with the spoof plasmon polaritons in these cases.

To do this, we consider Floquet–Bloch conditions in the xy-plane: $\mathbf{E}(x + d, y + d, z) = \mathbf{E}(x, y, z,)\exp(\mathrm{i}(kx + ky)d)$ (and similarly for the magnetic field) with $\mathbf{k} = (kx, ky)$ the Bloch vector that describes the first Brillouin zone ΓXM in the reciprocal space ($\Gamma = (0, 0)$, $X(\pi/d, 0)$, $M(\pi/d, \pi/d)$), where d is the pitch of the array in the physical space. We consider a small volume of vacuum above and below the structured metal, and periodic conditions in the z-direction, since CST does not allow for a combination of Floquet–Bloch conditions and perfectly matched layers (this seems to be mainly due to the fact that this would involve search of complex eigenfrequencies associated with so-called quasi-modes [33], which cannot be done in CST). We numerically checked the convergence of eigenfrequencies versus depth of the structured metal (the deeper the metal, the lower the cut-off frequency). For the plasmonic crystal, which consists of a perfect metal with dry sand inclusions, we finally obtain the dispersion of the fundamental mode as shown in figure 18. The SfPP propagates on the structured metal surface below a cut-off frequency of nearly 10 GHz (we numerically find 9.89 GHz) as requested.

In order to confirm the existence of the SfPP below 10 GHz, we now consider a finite plasmonic crystal with dimensions $L = 1 = 120$ mm and $h = 40$ mm illuminated with an electric source over a large range of microwave frequencies (between 5 GHz and 7 GHz) well below the cut-off frequency of 10 GHz. We show in figure 19 the result of CST simulations for the real part of the electric field component Ez (view from top for a plane located 1 mm above the crystal). The side view is shown in figure 20. The SfPP is clearly visible in figure 19 at the aforementioned frequencies: it propagates with almost circular wavefronts in the xy-plane, which shows that the effective medium is indeed isotropic in this plane. For frequencies higher than 10 GHz, the electromagnetic wave which is evanescent along the dielectric (sand)

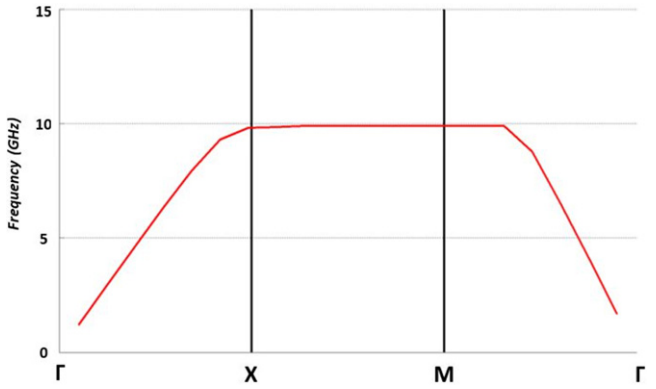

Figure 18. Numerical simulation of the dispersion diagram for a spoof plasmon for dry sand inclusions with a square cross-section of sidelength $a = 7.9$ mm, evenly spaced along a square lattice of pitch $d = 10$ mm with a perfect metal of infinite transverse dimensions and depth $h = 40$ mm. SfPP propagates below the cut-off frequency 10 GHz.

waveguide axes as clearly seen in figure 20, stops propagating in the xy-plane and propagates through the dielectric waveguides (the field remains of course evanescent in the perfect metal regions), that is, along the z-direction.

For the realization of the plasmonic crystal, we use a metallic grid (11 × 11 cells) consisting of aluminium tubes with a depth of 40 mm and with a square cross section of smaller and larger sidelengths 8 mm and 10 mm filled with dry sand. We show in figure 20 a comparison between the real part of Ez fields obtained from the simulations (upper panels) and the results of experimental measurements (lower panels) at 5 GHz, 6 GHz and 7 GHz (from left to right) with a network analyzer. One can clearly see the surface wave nature of the electric field, which propagates along the (horizontal) xy-plane and is evanescent along the (vertical) z-direction.

5.2. A plasmonic fisheye with polystyrene and sand

We are now in a position to propose a practical implementation of a fisheye lens for SfPPs. In figure 21 we show some numerical simulations (CST Microwave Studio) for an electric source generating SfPPs at 5 GHz (upper right), 6 GHz (lower left) and 7 GHz (lower right). The schematic diagram of the fisheye is shown in the upper left panel of figure 21. The symmetry of the field with respect to a line passing through the centre of the fisheye is noted, and is a hallmark of the stereographically projected light rays of the virtual sphere underpinning the design of the lens as shown in figure 1. We numerically checked that fisheye lensing is actually achieved from 4 GHz to 8 GHz so it is a broadband effect (the only constraints being that the frequency is not too small or too large so that the fisheye is not of sub-wavelength overall size, and that its structural details remain smaller than the wave wavelength for effective medium theory to remain valid).

We finally show in figure 22 the experimental proof of concept of the plasmonic fisheye. The left panels show a photo of the mould of the fisheye in the upper panel. The lower panel depicts a 3D view of the Ez field computed on the outer boundaries of the fisheye lens and on those of the

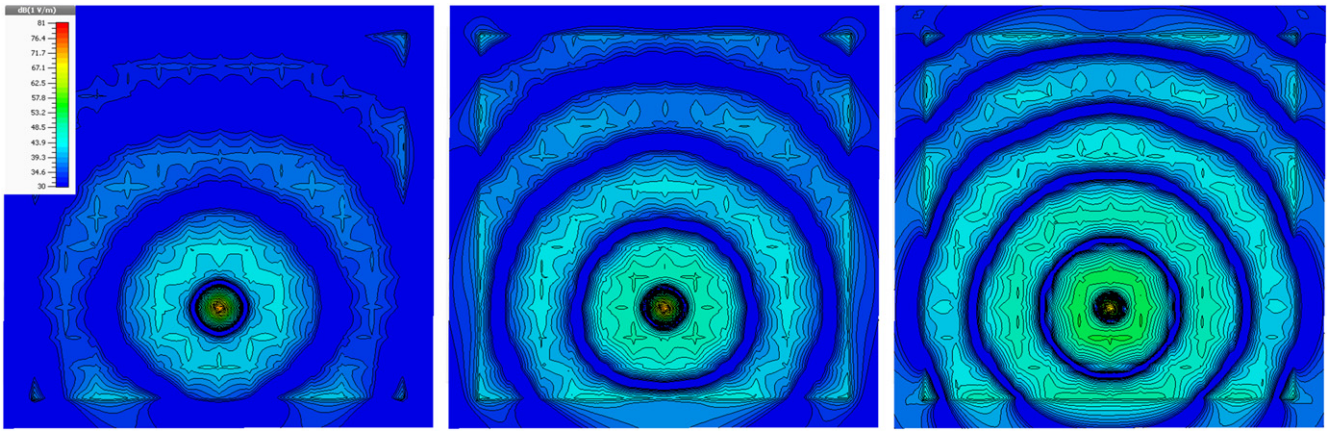

Figure 19. Slice along *xy* taken 1 mm above the structured metal. Top view of real part of electric field *Ez* for an electric source generating an SfPP at frequency (from left to right) 5 GHz, 6 GHz and 7 GHz on the same plasmonic crystal as in figure 18 but with finite dimensions $L = l = 120$ mm and $h = 40$ mm. Colour scale is in dB.

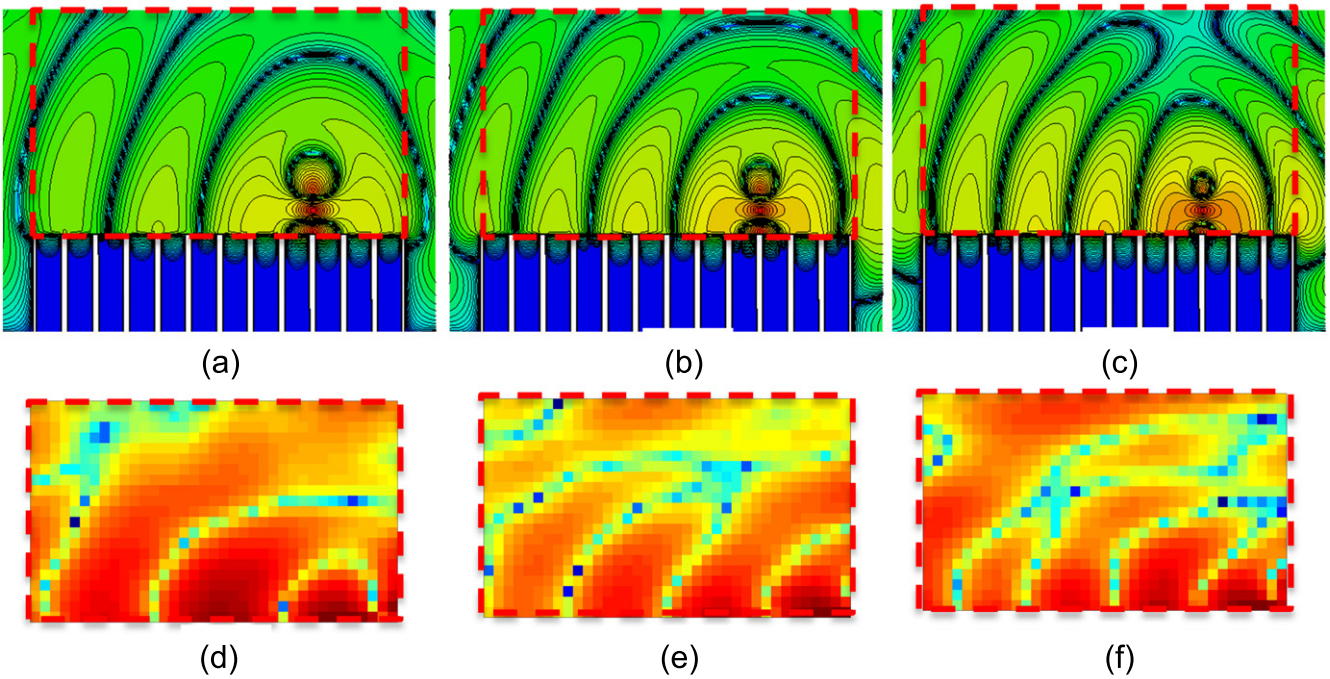

Figure 20. Numerical results (a)–(c) versus experimental measurements (d)–(f) of spoof plasmon polariton at 5 GHz (a), (d), 6 GHz (b), (e) and 7 GHz (c), (f). Maps of real part of *Ez* in the *xz*-plane above the metal with colour scales in dB (20 log Real(*Ez*)).

plasmonic crystal (the *Ez* field is zero on the latter since it is perfect metal). This lower panel also shows the plane, located 1 mm above the fisheye, along which we take a slice of the *Ez* field. In the middle panel, experimental measurements performed with the same setup as in figure 20 clearly demonstrate the lensing effect at 5 GHz. Numerical simulations (see right panel) are in very good agreement with experiments. One limitation of our device is that over the range of working frequencies, the plasmonic crystal is barely large enough to accommodate both the source and the image. However, our experimental results are a conclusive validation of the theoretical proposal of open plasmonic fisheye as shown in figure 16. Other improvements might consist in making the fisheye lying atop the structured metal thicker. One might also wish to place the electric source within the fisheye and look at lensing in a closed fisheye lens, which requires adding a perfect metal cavity around the fisheye (for instance with an aluminium sheet), and in this case one might achieve similar features as in figure 17. We believe that our proof of concept of a plasmonic fisheye can be easily translated into other gradient index lenses, such as Luneburg and Eaton lenses.

6. Concluding remarks and perspectives in other wave areas

In this paper, we reviewed some properties of transformational plasmonics and proposed some designs of cyclic

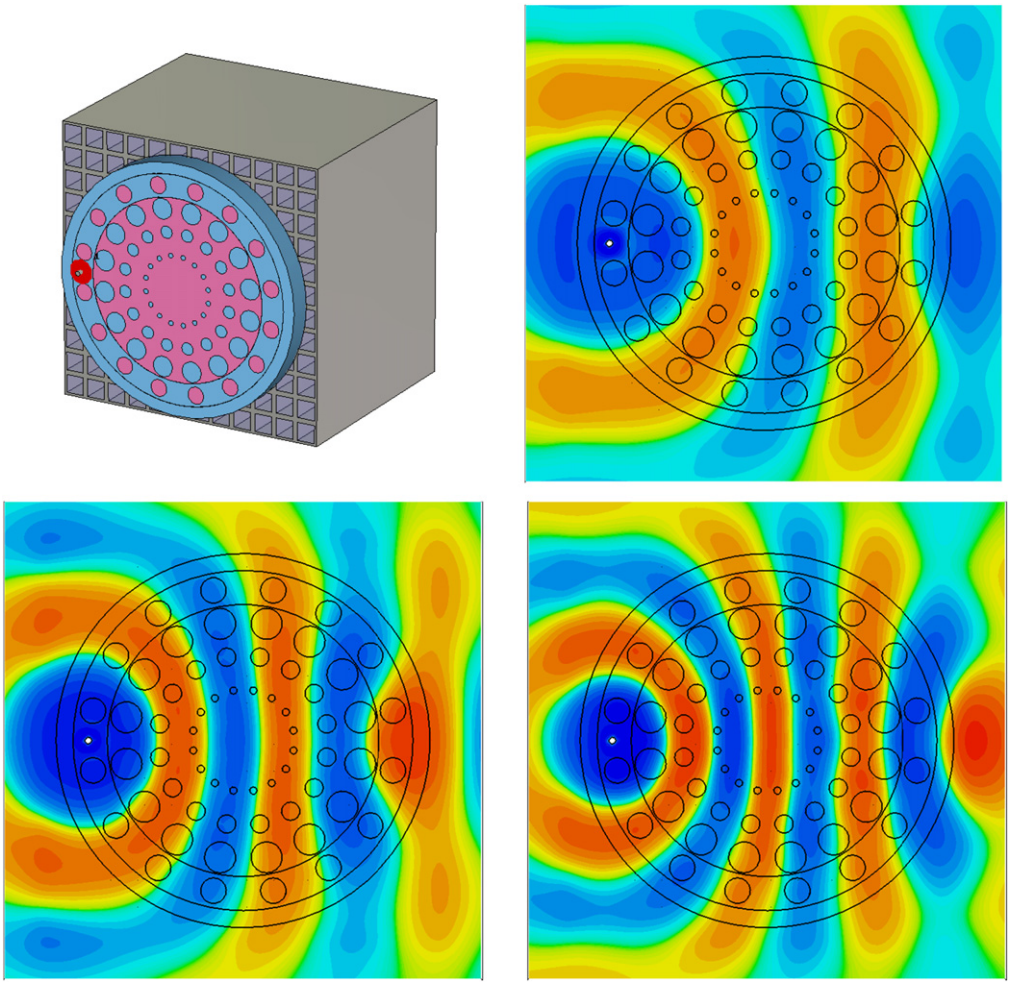

Figure 21. Schematic of fisheye and numerical results for spoof plasmon polariton. (Upper left) Pink regions shall be filled with sand (relative permittivity of 3.4) whereas blue regions are filled with polystyrene (of similar permittivity to air). (Upper right) Real part of Ez at 5 GHz. (Lower left) Re(Ez) at 6 GHz. (Lower right) Re(Ez) at 7 GHz. Colour scale is linear.

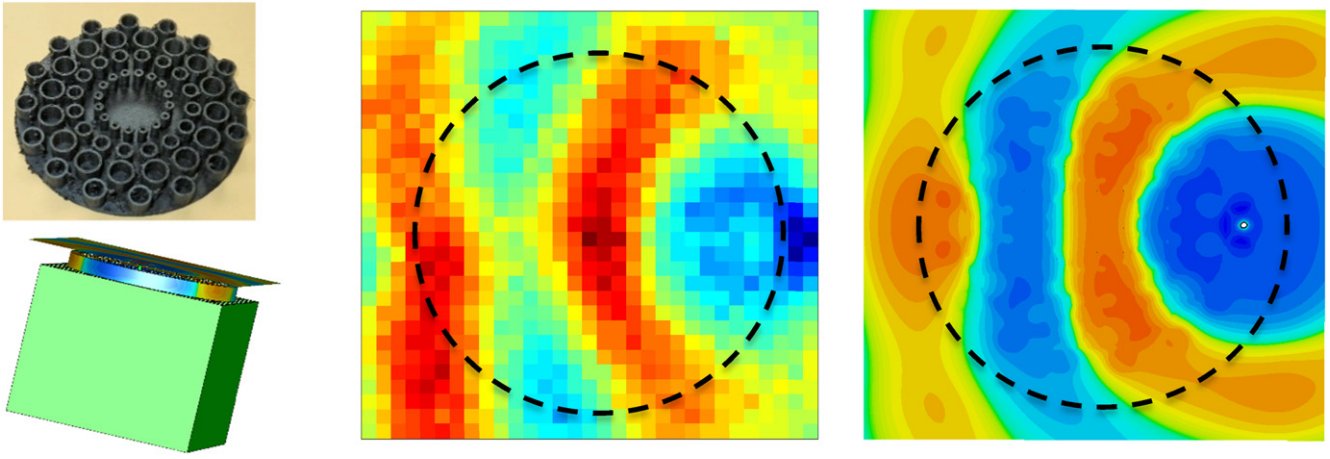

Figure 22. Experimental results on plasmonic fisheye lens. (Left) Photo of fisheye's mould fabricated with a 3D printer (top view) where the cylinders have a coating 1 mm thick and 3D view of the CST simulation with the plane where we slice Ez field. (Middle) Top view of real part electric field Ez measured at 5 GHz with the source on the right and its image on the left with the boundary of fisheye marked as a dashed line. (Right) Computed Re(Ez).

concentrators, carpets and cloaks. We investigated the physics of spoof plasmon polaritons introduced by Pendry, Martin-Moreno and Garcia-Vidal in 2004 [2] at a perfect metal surface structured with sand with a fisheye lens lying atop, the latter achieving a spatially varying refractive index with a combination of air and sand. We experimentally demonstrated a prototype of a plasmonic fisheye in the microwave regime between 5 GHz and 7 GHz. To conclude this review article, we would like to point out some connections between these small-scale experiments for electromagnetic waves and large-scale experiments conducted in structured soils [6]. Rayleigh waves behave in many ways like SfPPs; at least from a mathematical standpoint they have a similar form (notably the exponential decrease of the displacement field in the plane perpendicular to the air–soil interface). We thus propose that one might test seismic metamaterials at a laboratory scale using analogies between plasmonics and geophysics, for instance in the microwave regime where devices such as cloaks are easier to test [36] than in optics. As a first prediction, we believe that surface polariton waves analogous to SfPPs observed on thin metal stripes almost 15 years ago [37] could be observed in the form of Rayleigh waves in sols structured with trenches. One can also envision the testing of a variety of transformation optics–based plasmonic metamaterials (e.g. cloaks, concentrators, lenses [38–55]) and translate the most promising devices in the realm of transformation seismology. This is in essence what our group is currently doing in collaboration with Imperial College London (group of Richard Craster), with the Earth Science Institute ISTerre in Grenoble (group of Philippe Roux) and in partnership with the civil engineering Ménard Company in Lyon (group of Stéphane Brûlé). Moreover, similar studies are being led for the control of surface ocean waves, and here again useful analogies can be drawn with transformation plasmonics in order to design e.g. dykes for the protection of coastlines (based on surface water wave carpets, beam shifters and cloaks [56–59] whose designs are indeed reminiscent of plasmonic metamaterials). The versatility of transformation optics techniques introduced by John Pendry, David Schurig and David Smith in 2006 therefore represents not only a shift in electromagnetic paradigm, but also in acoustics, hydrodynamics and elastodynamics [59]. Analogues of spoof plasmons could be found in many wave areas where interfaces are structured at a subwavelength scale using effective medium theories [16, 60] that unveil exotic plasmonic behaviors such as cloaking [61, 62] and extreme control of light notably in metamaterials nanotips [63, 64]. The knowledge gained in metamaterial surfaces over the past few years thanks to the advent of plasmonic metamaterials will certainly have deep implications in other disciplines, notably in civil and maritime engineering.

Acknowledgements

R A, S E, and S G are thankful for a PEPS INSIS/CNRS funding through project CLOAK EXTERNE. S G acknowledges funding from ERC through the project ANAMORPHISM. Research conducted within the context of the International Associated Laboratory ALPhFA: Associated Laboratory for Photonics between France and Australia. This work has been carried out thanks to the support of the A*MIDEX project (no. ANR-11-IDEX-0001-02) funded by the Investissements d'Avenir French Government program, managed by the French National Research Agency (ANR).

References

[1] Lamb H 1898 On the reflection and transmission of electric waves by a metallic grating *Proc. Lond. Math. Soc.* **29** 523–44
[2] Pendry J B, Martin-Moreno L and Garcia-Vidal F J 2004 Mimicking surface plasmons with structured surfaces *Science* **305** 847–8
[3] Hibbins A P, Evans B R and Sambles J R 2005 Experimental verification of designer surface plasmons *Science* **308** 670–2
[4] Maier S A 2007 *Plasmonics: Fundamentals and Applications* (Berlin: Springer)
[5] Sarid D and Challener W 2010 *Modern Introduction to Surface Plasmons* (Cambridge: Cambridge University Press)
[6] Brûlé S, Javelaud E, Enoch S and Guenneau S 2014 Experiments on seismic metamaterials: moulding surface waves *Phys. Rev. Lett.* **112** 133901
[7] Li J and Pendry J B 2008 Hiding under the carpet: a new strategy for cloaking *Phys. Rev. Lett.* **101** 203901
[8] Maxwell J C 1854 *Cambridge Dublin Math. J.* **9** 9–11
[9] Luneburg R K 1944 *Mathematical Theory of Optics* (Providence, RI: Brown University) pp 189–213
[10] Kadic M, Guenneau S and Enoch S 2010 Transformational plasmonics: cloak, concentrator and rotator for SPPs *Opt. Express* **18** 12027–32
[11] Huidobro P A, Nesterov M L, Martin-Moreno L and García-Vidal F J 2010 Transformation optics for plasmonics *Nano Lett.* **10** 1985–90
[12] Liu Y, Zentgraf T, Bartal G and Zhang X 2010 Transformational plasmon optics *Nano Lett.* **10** 1991–7
[13] Renger J, Kadic M, Dupont G, Aćimović S S, Guenneau S, Quidant R and Enoch S 2010 Hidden progress: broadband plasmonic invisibility *Opt. Express* **18** 15757–68
[14] Kadic M, Guenneau S, Enoch S, Huidobro P A, Martin-Moreno L, García-Vidal F J, Renger J and Quidant R 2012 Transformation plasmonics *Nanophotonics* **1** 54–61
[15] Pendry J P, Schurig D and Smith D R 2006 Controlling electromagnetic fields *Science* **312** 1780–12
[16] Landauer R 1978 Electrical conductivity in inhomogeneous media *AIP Conf. Proc.* **40** 2–45
[17] Guenneau S and Zolla F 2000 Homogenization of three-dimensional finite photonic crystals *Prog. Electromagn. Res.* **27** 91–127
[18] Maystre D 1982 General study of grating anomalies from electromagnetic surface modes *Electromagnetic Surface Modes* ed A D Boardman (New York: Wiley)
[19] Pendry J B, Holden A T, Stewart W J and Youngs I 1996 Extremely-low-frequency plasmons in metallic mesostructures *Phys. Rev. Lett.* **25** 4773
[20] Felbacq D and Bouchitte G 1997 Homogenization of a set of parallel fibres *Waves Random Media* **7** 245–56
[21] Pendry J B, Holden A J, Robbins D J and Stewart W J 1998 Low frequency plasmons in thin-wire structures *J. Phys. Condens. Matter* **10** 4785–09

[22] Smith D R, Vier D C, Koschny T and Soukoulis C M 2005 Electromagnetic parameter retrieval from inhomogeneous metamaterials *Phys. Rev.* E **71** 036617
[23] Belov P A, Hao Y and Sudhakaran S 2006 Subwavelength microwave imaging using an array of parallel conducting wires as a lens *Phys. Rev.* B **73** 033108
[24] Pendry J B 2000 Negative refraction makes a perfect lens *Phys. Rev. Lett.* **85** 3966–9
[25] Leonhardt U 2009 Perfect imaging without negative refraction *New J. Phys.* **11** 093040
[26] Blaikie R J 2010 Comment on 'Perfect imaging without negative refraction' *New J. Phys.* **12** 058001
[27] Sun F 2010 Can Maxwell's fish eye lens really give perfect imaging? II. The case with passive drains *Prog. Electromagn. Res.* **108** 307–22
[28] Guenneau S, Diatta A and McPhedran R C 2010 Focusing: coming to the point in metamaterials *J. Mod. Opt.* **57** 511–27
[29] Ma Y G, Sahebdivan S, Ong C K, Tyc T and Leonhardt U 2011 Evidence for subwavelength imaging with positive refraction *New J. Phys.* **13** 033016
[30] Merlin R 2011 Maxwell's fish-eye lens and the mirage of perfect imaging *J. Opt.* **13** 024017
[31] de Rosny J and Fink M 2002 Overcoming the diffraction limit in wave physics using a time-reversal mirror and a novel acoustic sink *Phys. Rev. Lett.* **89** 124301
[32] Lefebvre G, Dubois M, Beauvais R, Achaoui Y, Kiri Ing R, Guenneau S and Sebbah P 2015 Experiments on Maxwell's fish-eye dynamics in elastic plates *Appl. Phys. Lett.* **106** 024101
[33] Vial B, Zolla F, Nicolet A and Commandré M 2014 Quasimodal expansion of electromagnetic fields in open two-dimensional structures *Phys. Rev.* A **89** 023829
[34] Georget E, Abdeddaim R and Sabouroux P 2014 A quasi-universal method to measure the electromagnetic characteristics of usual materials in the microwave range *C. R. Phys.* **15** 448–57
[35] Sabouroux P and Ba D 2011 Epsimu, a tool for dielectric properties measurement of porous media: Application in wet granular materials characterization *Prog. Electromagn. Res.* B **29** 191–207
[36] Edwards B, Alù A, Silveirinha M G and Engheta N 2009 Experimental verification of plasmonic cloaking at microwave frequencies with metamaterials *Phys. Rev. Lett.* **103** 153901
[37] Weeber J-C, Krenn J R, Dereux A, Lamprecht B, Lacroute Y and Goudonnet J P 2001 Near-field observation of surface plasmon polariton propagation on thin metal stripes *Phys. Rev.* B **64** 045411
[38] Moreno E, Rodrigo S G, Bozhevolnyi S I, Martín-Moreno L and García-Vidal F J 2008 Guiding and focusing of electromagnetic fields with wedge plasmon polaritons *Phys. Rev. Lett.* **100** 023901
[39] Ramakrishna S A, Mandal P, Jeyadheepan K, Shukla N, Chakrabarti S, Kadic M, Enoch S and Guenneau S 2011 Plasmonic interaction of visible light with gold nanoscale checkerboards *Phys. Rev.* B **84** 245424
[40] Wood J J, Tomlinson L A, Hess O, Maier S A and Fernández-Domínguez A I 2012 Spoof plasmon polaritons in slanted geometries *Phys. Rev.* B **85** 075441
[41] Zayats A V, Smolyaninov I I and Maradudin A A 2005 Nano-optics of surface plasmon polaritons *Phys. Rep.* **408** 131–314
[42] Kildishev A V, Cai W, Chettiar U K and Shalaev V M 2008 Transformation optics: approaching broadband electromagnetic cloaking *New J. Phys.* **10** 115029
[43] Baumeier B, Leskova T A and Maradudin A A 2009 Cloaking from surface plasmon polaritons by a circular array of point scatterers *Phys. Rev. Lett.* **103** 246803
[44] Gabrielli L H, Cardenas J, Poitras C B and Lipson M 2009 Silicon nanostructure cloak operating at optical frequencies *Nat. Photonics* **3** 461–3
[45] Valentine J, Li J, Zentgraf T, Bartal G and Zhang X 2009 An optical cloak made of dielectrics *Nat. Mater.* **8** 568–71
[46] Ergin T, Fischer J and Wegener M 2011 Optical phase cloaking of 700 nm light waves in the far field by a three-dimensional carpet cloak *Phys. Rev. Lett.* **107** 173901
[47] Huidobro P A, Nesterov M L, Martín-Moreno L and García-Vidal F J 2011 Moulding the flow of surface plasmons using conformal and quasiconformal mappings *New J. Phys.* **13** 033011
[48] Kadic M, Dupont G, Chang T-M, Guenneau S and Enoch S 2011 Curved trajectories on transformed metal surfaces: beam-splitter, invisibility carpet and black hole for surface plasmon polaritons *Photonics Nanostruct. Fundam. Appl.* **9** 302–7
[49] Alu A and Engheta N 2005 Achieving transparency with plasmonic and metamaterial coatings *Phys. Rev.* E **72** 016623
[50] Nicorovici N A, Milton G W, McPhedran R C and Botten L C 2007 Quasistatic cloaking of two-dimensional polarizable discrete systems by anomalous resonance *Opt. Express* **15** 6314–23
[51] Kadic M, Dupont G, Guenneau S and Enoch S 2007 Controlling surface plasmon polaritons in transformed coordinates *J. Mod. Opt.* **58** 994–1003
[52] Kadic M, Guenneau S, Enoch S and Ramakrishna S A 2011 Plasmonic space folding: focusing surface plasmons via negative refraction in complementary media *ACS Nano* **5** 6819–25
[53] Vakil A and Engheta N 2011 Transformation optics using graphene *Science* **332** 1291–4
[54] Landy N and Smith D R 2013 A full-parameter unidirectional metamaterial cloak for microwaves *Nat. Mater.* **12** 25–8
[55] Yao K and Liu Y 2014 Plasmonic metamaterials *Nanotechnol. Rev.* **3** 177–210
[56] Farhat M, Enoch S, Guenneau S and Movchan A B 2008 Broadband cylindrical acoustic cloak for linear surface waves in a fluid *Phys. Rev. Lett.* **101** 134501
[57] Berraquero C P, Maurel A, Petitjeans P and Pagneux V 2013 Experimental realization of a water-wave metamaterial shifter *Phys. Rev.* E **88** 051002
[58] Dupont G, Kimmoun O, Molin B, Guenneau S and Enoch S 2015 Numerical and experimental study of an invisibility carpet in a water channel *Phys. Rev.* E **91** 023010
[59] Kadic M, Bückmann T, Schittny R and Wegener M 2015 Experiments on cloaking in optics, thermodynamics and mechanics *Phil. Trans. R. Soc.* A **373** 20140357
[60] Sihvola A 1999 *Electromagnetic Mixing Formulas and Applications* (London: Institution of Electrical Engineers)
[61] Mühlig S, Farhat M, Rockstuhl C and Lederer F 2011 Cloaking dielectric spherical objects by a shell of metallic nanoparticles *Phys. Rev.* B **83** 195116
[62] Monti A, Bilotti F and Toscano A 2011 Optical cloaking of cylindrical objects by using covers made of core–shell nanoparticles *Opt. Lett.* **36** 4479–81
[63] Rockstuhl C, Simovski C R, Tretyakov S A and Lederer F 2009 Metamaterial nanotips *Appl. Phys. Lett.* **94** 113110
[64] Muhlig S, Rockstuhl C, Pniewski J, Simovski C R, Tretyakov S A and Lederer F 2010 Three-dimensional metamaterial nanotips *Phys. Rev.* B **81** 075317